Selective asymmetric gate control of the Rashba spin-orbit coupling in GaInAs/AlInAs stepped wells

Qingxuan Wang,[1] Hao Yang,[1] and Jiyong Fu[1,2,*]

[1]*Department of Physics, Qufu Normal University, 273165 Qufu, Shandong, China*

[2]*Instituto de Física, Universidade de Brasília, Brasília, Distrito Federal 70919-970, Brazil*

(Received 28 March 2020; revised manuscript received 2 May 2020; accepted 6 May 2020; published 2 June 2020)

Resorting to ordinary GaInAs/AlInAs stepped quantum wells subjected to an external gate, which allows for adjusting the well symmetry and electron occupancy, we demonstrate that the Rashba spin-orbit (SO) strengths of the first (α_1) and second (α_2) subbands exhibit opposite gate dependence, triggered by the *inner* barrier, of which the structural potential energy for electrons is *sandwiched* between energy levels of two subbands. This opens a route towards selective and opposite SO control, greatly fascinating for spintronic applications. Moreover, we find that α_1 and α_2 may have opposite signs, in favor of hosting topological matter of persistent skymion lattice in conventional semiconductor heterostructures that we recently proposed [J. Y. Fu, P. H. Penteado, M. O. Hachicya, D. Loss, and J. C. Egues, Phys. Rev. Lett. **117**, 226401 (2016)]. Finally, while the interband Rashba term (η) is found to be essentially gate independent, it may lead to the energy dispersion anticrossing or maintaining crossing, depending on intraband Rashba couplings.

DOI: 10.1103/PhysRevB.101.245403

I. INTRODUCTION

The spin-orbit (SO) interaction, which couples electron spin and momentum via an effective magnetic field, is a key issue in the field of spintronics, as it provides a unique handle for electrical manipulation of the spin magnetic moment [1,2]. The SO coupling also lifts spin degeneracy and may mix spin states, thus giving rise to spin hybridization gaps and nontrivial spin textures [3,4]. Spin-orbit effects lie at the core of topological phenomena in diverse fields of condensed matter, such as topological insulators [5], Majorana fermions [6,7], and Weyl semimetals [8]. Moreover, the SO coupling is a central ingredient leading to *spin-valley locking* in 2D materials of transition metal dichalcogenides [9–11]. Our recent proposals of persistent skyrmion lattice [12] and stretchable spin helix [13] and its symmetry breaking [14] also indicate the important role of SO effects in semiconductor nanostructures.

In semiconductor nanostructures, the SO effects usually have two dominant contributions, i.e., the Rashba [15] and Dresselhaus [16] terms, arising from the structural and bulk inversion asymmetries, respectively. While the Dresselhaus coupling mainly depends on the quantum confinement [13,17,18], the Rashba coupling can be electrically controlled by using an external bias, thus facilitating spin manipulation [13,19–21]. As a consequence, the Rashba effect is often used in proposed spintronic devices, e.g., spin-field [22–24] and spin-Hall effect [25,26] transistors. Extensive studies have been devoted to the electrical spin control by resorting to the Rashba effect in semiconductor heterostructures including single [13,27], double [27,28], and even mutiple wells [29,30] with either one or two occupied electron subbands. Furthermore, semiconductors such as GaAs, InAs, or InSb, offer various strengths of SO couplings [13,19,27,31,32] and are thus suitable for a broad range of spintronic applications, making this subject extraordinarily profound.

Here we consider ordinary GaInAs/AlInAs stepped quantum wells [Fig. 1(a)], in which the SO term is at least 1 order of magnitude larger than that in GaAs-based wells. The stepped wells have diverse applications especially about interband effects [33,34] and allow for considering an interesting geometry in which the structural potential energy for electrons due to the *inner* barrier is *sandwiched* between energy levels

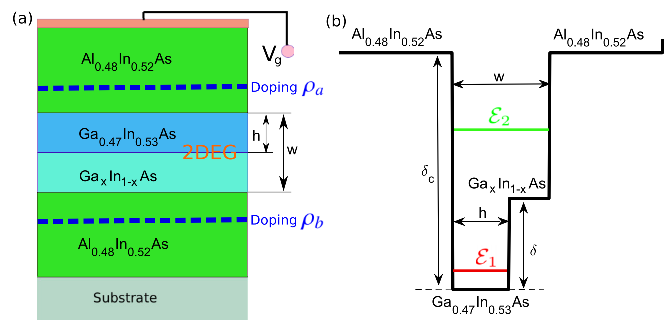

FIG. 1. (a) Schematic diagram of a GaInAs/AlInAs stepped quantum well, with w and $(w-h)$ denoting the width of the overall well [2DEG, two-dimensional electron gases] and of the inner stepped barrier ($Ga_xIn_{1-x}As$), respectively. The dashed (blue) regions inside the outer barriers ($Al_{0.48}In_{0.52}As$) stand for doping layers with doping density ρ_a and ρ_b, and V_g refers to an external gate potential. (b) Schematic illustration of the structural potential profile of the stepped well in panel (a), where δ_c (δ) denotes the outer (inner) band offset and $\mathcal{E}_1$ ($\mathcal{E}_2$) is the subband energy level below (above) the inner barrier.

*yongjf@qfnu.edu.cn

 ©2020 American Physical Society

of the first ($\mathcal{E}_1$) and second ($\mathcal{E}_2$) subbands [Fig. 1(b)]. Stepped wells also embrace an *intrinsic* structural inversion asymmetry (SIA) due to the inner barrier. With the help of an external gate potential (V_g), which allows for a simultaneous tuning of the electron occupancy and SO strength [13,14], we observe selective asymmetric gate control of the Rashba SO couplings.

We demonstrate that the strengths of the Rashba SO couplings of the two subbands, i.e., α_1 and α_2, exhibit entirely opposite gate dependence [Fig. 2(d) (dotted curves) and Figs. 3(a) and 3(b)], because of the inner barrier, of which the structural potential energy for electrons is *sandwiched* between the two-band energy levels. This opens a route towards selective and opposite SO control, greatly fascinating for spintronic devices. Moreover, we observe that α_1 and α_2 may have opposite signs, in favor of hosting topological matter of persistent skyrmion lattice formed by conventional 2D electron gases (2DEGs) that we recently put forward [12]. As for the interband SO coupling (η), we find that it is almost independent of the external gate [Fig. 4(a)], while it may lead to the energy dispersion anticrossing [Fig. 4(c)] or maintaining crossing [Fig. 4(b)], depending on intraband Rashba terms.

This paper is organized as follows. In Sec. II, starting from the 3D Hamiltonian for conduction electrons, we derive its effective 2D form in our wells. In Sec. III, we show expressions of the Rashba SO coefficents of both intraband and interband terms. In Sec. IV, we present our self-consistent results and discussion. We summarize our main findings in Sec. V.

II. MODEL HAMILTONIANS FROM THREE DIMENSIONS TO TWO DIMENSIONS

We consider stepped quantum wells grown along the $z||[001]$ direction. Starting from the 8×8 Kane model [36,37] with both conduction and valence bands, one obtains *via* the folding down procedure [18,27] an effective three-dimensional (3D) Hamiltonian only for conduction electrons,

$$\mathcal{H}^{3D} = \frac{\hbar^2 k^2}{2m^*} - \frac{\hbar^2}{2m^*}\frac{\partial^2}{\partial z^2} + V(z) + \mathcal{H}_{\mathcal{R}}^{3D}, \quad (1)$$

where m^* is the electron effective mass and k is the in-plane electron momentum. The third term $V = V_w + V_g + V_d + V_e$ is the electron confining potential, which is determined self-consistently within the Poisson-Schrödinger Hartree approximation, with V_w being the structural potential (band offsets), V_g the external gate potential, V_d the doping potential, and V_e the electron Hartree potential [12,13,18,27]. The last term, $\mathcal{H}_{\mathcal{R}}^{3D} = \eta(z)(k_x\sigma_y - k_y\sigma_x)$, describes the Rashba SO interaction, with $\eta(z) = \eta_w\partial_z V_w + \eta_H\partial_z(V_g + V_d + V_e)$ determining the Rashba SO strength and $\sigma_{x,y,z}$ the spin Pauli matrices. The Rashba parameters η_w and η_H involve bulk quantities of materials [18,27,38].

Now we are ready to define an effective 2D model from the 3D Hamiltonian above. We first determine (self-consistently) the spin-degenerate eigenvalues $\varepsilon_{\mathbf{k}\nu} = \mathcal{E}_\nu + \hbar^2k^2/2m^*$ and the corresponding eigenspinors $|\mathbf{k}\nu\sigma\rangle = |\mathbf{k}\nu\rangle\otimes|\sigma\rangle$ and $\langle\mathbf{r}|\mathbf{k}\nu\rangle = \exp(i\mathbf{k}\cdot\mathbf{r})\psi_\nu(z)$ of the well in the absence of SO interaction. Here we have defined $\mathcal{E}_\nu$ (ψ_ν), $\nu = 1$ and 2, as the νth quantized energy level (wave function) and $\sigma =\uparrow$ and $\downarrow$ as the electron spin component along the z direction. Then the effective 2D Rashba model with two subbands in the coordinate system $[x||(100), y||(010)]$ under the basis set $\{|\mathbf{k}1\uparrow\rangle, |\mathbf{k}1\downarrow\rangle, |\mathbf{k}2\uparrow\rangle, |\mathbf{k}2\downarrow\rangle\}$ reads

$$\mathcal{H}^{2D} = \left(\frac{\hbar^2k^2}{2m^*} + \mathcal{E}_+\right)\mathbb{1}\otimes\mathbb{1} - \mathcal{E}_-\tau_z\otimes\mathbf{1} + \mathcal{H}_{\mathcal{R}}^{2D}, \quad (2)$$

with $\mathcal{E}_\pm = (\mathcal{E}_2 \pm \mathcal{E}_1)/2$, $\mathbb{1}$ being the 2×2 identity matrix in spin or orbital (subband)] subspaces, and $\tau_{x,y,z}$ being the Pauli ("pseudospin") matrices acting within the orbital subspace. The term $\mathcal{H}_{\mathcal{R}}^{2D}$ describes the Rashba SO contributions in terms of intra- and intersubband SO fields $\mathbf{\Omega}_{SO}^{\nu}$ and $\mathbf{\Omega}_{SO}^{12}$, respectively,

$$\mathcal{H}_{\mathcal{R}}^{2D} = \sum_{\nu=1,2}\left[\tau_\nu\otimes\boldsymbol{\sigma}\cdot\mathbf{\Omega}_{SO}^{\nu} + \tau_x\otimes\boldsymbol{\sigma}\cdot\mathbf{\Omega}_{SO}^{12}\right], \quad (3)$$

with $\tau_{1,2} = (\mathbf{1}\pm\tau_z)/2$. The intrasubband SO field reads

$$\mathbf{\Omega}_{SO}^{\nu} = \alpha_\nu k[\sin(\theta)\hat{\mathbf{x}} - \cos(\theta)\hat{\mathbf{y}}], \quad (4)$$

and the intersubband SO field is

$$\mathbf{\Omega}_{SO}^{12} = \eta k[\sin(\theta)\hat{\mathbf{x}} - \cos(\theta)\hat{\mathbf{y}}], \quad (5)$$

with θ being the angle between $\mathbf{k}$ and the x axis.

III. RASHBA COEFFICIENTS

The Rashba SO coefficients α_ν and η, Eqs. (4) and (5), can be cast as the expectation values $\langle\ldots\rangle$ of the weighted derivatives of the potential contributions,

$$\eta_{\nu\nu'} = \langle\psi_\nu|\eta_w\partial_z V_w + \eta_H\partial_z(V_g + V_d + V_e)|\psi_{\nu'}\rangle, \quad (6)$$

with $\alpha_\nu \equiv \eta_{\nu\nu}$ and $\eta \equiv \eta_{12}$. Note that the intraband Rashba term α_ν can be written in terms of several constituent contributions, i.e., $\alpha_\nu = \alpha_\nu^g + \alpha_\nu^d + \alpha_\nu^e + \alpha_\nu^w$, with $\alpha_\nu^g = \eta_H\langle\psi_\nu|\partial_z V_g|\psi_\nu\rangle$ being the gate contribution, $\alpha_\nu^d = \eta_H\langle\psi_\nu|\partial_z V_d|\psi_\nu\rangle$ the doping contribution, $\alpha_\nu^e = \eta_H\langle\psi_\nu|\partial_z V_e|\psi_\nu\rangle$ the electron Hartree contribution, and $\alpha_\nu^w = \eta_w\langle\psi_\nu|\partial_z V_w|\psi_\nu\rangle$ the structural contribution. Similarly, the interband Rashba term $\eta = \eta^g + \eta^d + \eta^e + \eta^w$. For convenience, we also use $\alpha_\nu^{g+d} = \alpha_\nu^g + \alpha_\nu^d$ and $\eta^{g+d} = \eta^g + \eta^d$. Even though α_ν and η comprise seemingly independent contributions, we note that each of them depends on the total potential *via* the self-consistent wave function; see the Supplemental Material [39].

IV. RESULTS AND DISCUSSION

We first introduce our system and relevant parameters adopted. Then, we show our self-consistent calculation on SO couplings. The random Rashba SO contribution is also discussed.

A. System and parameters

We consider ordinary [001]-grown AlInAs/GaInAs stepped wells, as shown in Fig. 1(a), similar to the experimental samples of Ref. [40], with an inner barrier ($Ga_xIn_{1-x}As$ layer, $x \geqslant 0.47$) inserted in the well (2DEG) region. The overall 2DEG width is $w = 14$ nm, containing the

TABLE I. Correspondence between the inner offset δ [Fig. 1(b)] considered in Figs. 2–4 and the concentration x of the inner barrier ($Ga_xIn_{1-x}As$) layer [42]. A mapping between δ and the effective electron mass m^* of the $Ga_xIn_{1-x}As$ layer is also listed [42]. The units of δ and m^* are in eV and m_0 (bare electron mass), respectively.

δ	x	m^*
0	0.47	0.043
0.02	0.50	0.044
0.1	0.59	0.048

$Ga_{0.47}In_{0.53}As$ layer of width $h = 7$ nm and the inner barrier of width $(w - h) = 7$ nm. Two doping layers of width 6 nm sit 18 nm away from either side of the well, with the doping densities $\rho_a = \rho_b = 2.5 \times 10^{18}$ cm^{-3} for a symmetric doping condition. The temperature is 0.3 K, and the Fermi level in our self-consistent simulation is pinned at $\mathcal{E}_F = 200$ meV [41]. An external gate potential (V_g) is adopted for adjusting the electron occupancy and the symmetry of the well profile, and therefore the strength of the Rashba SO coupling.

Figure 1(b) shows a schematic of the structual potential of the layered system in Fig. 1(a). The outer offset is chosen as $\delta_c = 0.52$ eV [27,42], while the inner one δ is treated as a tunable parameter, equivalent to varying the composition (x) in the $Ga_xIn_{1-x}As$ layer. This allows for considering an interesting geometry, in which the structural potential energy for electrons due to the inner barrier is *sandwiched* between the energy levels of the two subbands [Fig. 1(b)]. For realistic considerations, we follow Ref. [42] and determine a mapping between the inner offset δ and the concentration x of the $Ga_xIn_{1-x}As$ layer for several values of δ involved in Figs. 2–4, as shown in Table I.

B. Self-consistent outcome

In Fig. 2(a), we show the zero-bias self-consistent potential and the two-subband wave function profiles of a stepped well in the *sandwich* geometry with $\delta = 0.1$ eV, for which the energy levels $\mathcal{E}_1$ and $\mathcal{E}_2$ are below and above the structural potential energy for the inner barrier, respectively, as indicated by the horizontal red and green lines inside the well [cf. Figs. 2(a) and 1(b)]. Due to the intrinsic SIA induced by the inner barrier, the first-subband electrons are apt to be localized on the left side of the well, while the second-subband electrons preferably reside in the right side (inner-barrier layer), as indicated by the electron distributions ψ_1 and ψ_2.

When the external bias is switched on, an external SIA, which electrons of the first and second subbands *feel* in stark contrast, is induced [see Fig. 2(b) for our self-consistent solutions at $V_g = 0.15$ eV]. First, with increasing V_g, the first-subband electrons experience an enhancement of SIA, while for the second subband the situation is the opposite [cf. dotted (black) and solid (blue) curves for the potential profile at $V_g = 0$ and 0.15 eV, respectively]. Second, the overall force fields due to the electron Hartree and gate plus doping potentials, i.e., $F_e + F_{g+d}$ with $F_{g+d} = F_g + F_d$, felt by the electrons of the two subbands have opposite signs, as indicated in Fig. 2(c) with black circles 1 and 2.

These self-consistent features of our wells in the sandwich geometry are helpful in elucidating our main findings. To systematically analyze our results, we first have a look at the usual scenario.

C. Usual scenario of Rashba control

The usual scenario corresponds to two trivial cases, in which the energy levels $\mathcal{E}_1$ and $\mathcal{E}_2$ are both below or both above the structural potential energy for the inner barrier. Without lack of generality, we look into the limit case of zero inner offset, as shown in Fig. 2(d) for $\delta = 0$. This configuration represents a trivial single well, thus the well is symmetric at $V_g = 0$, leading to vanishing zero-bias Rashba couplings for both subbands. When V_g differs from zero, we find that α_1 and α_2 exhibit similar gate dependence. Namely, they have the same sign and both increase in magnitude with growing V_g, as anticipated. Different strengths of α_1 and α_2 are attributed to the electron Hartree potential across the 2DEG region, which has the opposite effect in contributing to α_1 and α_2.

D. Opposite Rashba control

Now we turn to the sandwich geometry aforementioned in Figs. 2(a) and 2(b). In this scenario, the gate dependence of Rashba terms is shown in Fig. 2(d) with dotted curves for $\delta = 0.1$ eV. At $V_g = 0$, either α_1 or α_2 differs from zero due to the intrinsic SIA induced by the inner barrier, as opposed to the case of $\delta = 0$ (cf. dotted and solid curves). Remarkably, as V_g grows we observe that α_1 increases while α_2 decreases, indicating that α_1 and α_2 exhibit entirely opposite gate dependencies. This is in stark contrast to the usual scenario and opens a route towards opposite and selective Rashba control, greatly fascinating for spintronic applications. This feature may also bring about the concept of *spin-subband locking*, despite the lack of direct protection from the time reversal symmetry. Moreover, α_1 and α_2 have opposite signs and tend to become matched in magnitude with increasing V_g, favoring the formation of topological matter of persistent skyrmion lattice [12]. The inset shows in this scenario the second subband becomes empty at around $V_g = 0.16$ eV, as marked by the vertical (dotted) line.

The outcome of opposite Rashba control entirely comes from our self-consistent solutions: (i) the gate potential enhances the SIA felt by the first-subband electrons while it quenches the SIA for electrons of the second subband; (ii) the overall force fields felt by electrons of two subbands have opposite signs. From Eq. (6), it is straightforward that solution (i) leads to the opposite gate dependence of Rashba couplings and solution (ii) gives rise to opposite signs between α_1 and α_2.

To analyze further these features, in Fig. 3(a) [Fig. 3(b)], we show the Rashba couplings of the two subbands and the corresponding constituent contributions as a function of V_g. For the gate plus doping contribution, we find $\alpha_1^{g+d} = \alpha_2^{g+d}$ [cf. Figs. 3(a) and 3(b)]. This is because the force field F_{g+d} remains constant across the whole 2DEG region [Fig. 2(c)]. As opposed to α_ν^{g+d}, the electron Hartree contributions α_1^e and α_2^e instead have opposite signs since F_e on the left side of the well is opposite to that on the right side [Fig. 2(c)].

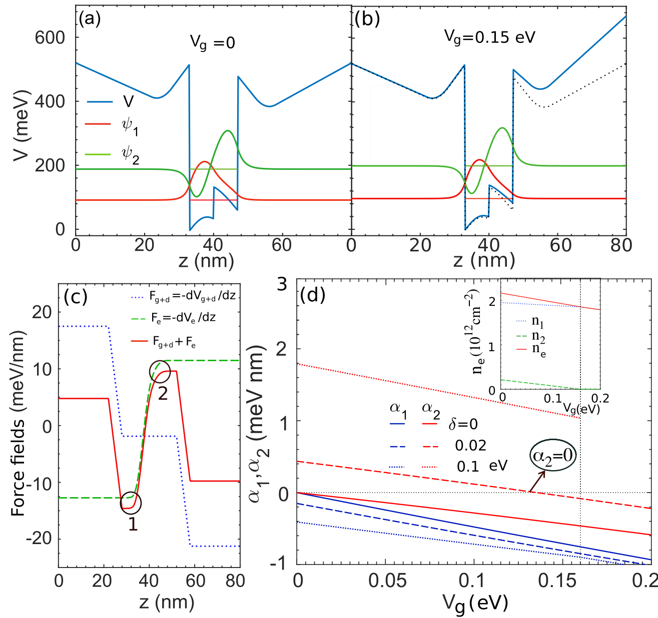

FIG. 2. (a) Self-consistent potential (V) and the corresponding wave function profiles of the first (ψ_1) and second (ψ_2) subbands for a AlInAs/GaInAs stepped well with $\delta = 0.1$ eV (see Fig. 1), at $V_g = 0$ (a) and 0.15 eV (b). The horizontal red (green) line inside the well indicates the energy level $\mathcal{E}_1$ ($\mathcal{E}_2$). The black (dotted) curve in panel (b) represents the potential in panel (a) for an eye-guiding comparison. (c) Force fields of F_e, F_{g+d} ($=F_g + F_d$), and the sum. Black circles 1 and 2 indicate corresponding force fields on the left and right sides of the well, respectively. (d) Rashba coefficients α_1 and α_2 as functions of V_g at $\delta = 0$, 0.02, and 0.1 eV. The vertical (dotted) line at $V_g = 0.16$ eV marks a transition from double- to single-electron occupancy. The inset shows how subband occupation varies with V_g.

Regarding the structural constituents, we find that α_1^w and α_2^w also have opposite signs, following from the combined effects of three interfaces of stepped wells. These analyses indicate the electron Hartree and structural contributions are the key constituents giving rise to the opposite Rashba control.

We should emphasize that we have assumed three interfaces share a common value for η_w, which in general should differ [13,18]. Moreover, although electrons are distributed throughout the well region [Figs. 2(a) and 2(b)], here we have assumed the same effective electron mass m^* across the inner barrier, following from a small distinction of it for the two materials inside the quantum well in the parameter range considered. Even at the largest inner offset of $\delta = 0.1$ eV that we consider [Fig. 2(d)], which corresponds to the inner barrier of $Ga_{0.59}In_{0.41}As$, the effective electron masses of the two layers forming the inner offset are m^* ($Ga_{0.59}In_{0.41}As$) $= 0.048m_0$ and m^* ($Ga_{0.47}In_{0.53}As$) $= 0.043m_0$ [42], respectively, with m_0 being the bare electron mass [see Table I and Fig. 1(b)]. By solving the Ben Daniel–Duke model [43], which takes into account layer-dependent m^* for our stepped wells, we obtain at $\delta = 0.1$ eV the zero-bias Rashba SO strengths $\alpha_1 = 0.2$ meV Å and $\alpha_2 = 2.1$ meV Å, as compared to 0.2 and 1.8 meV Å of the same effective mass approximation [Fig. 1(d)]. Note that for relatively larger values of δ that are not shown here, our calculations based on the Ben Daniel–Duke model [43] ensure that the fundamental feature of selective asymmetric gate control of the Rashba SO coupling remains the same.

E. Intermediate scenario: $\alpha_1 \neq 0, \alpha_2 = 0$

From the SO features of the usual scenario and of the sandwich geometry aforementioned, it is rational to conjecture that there may exist another interesting situation such that the inequality ($\alpha_1 \neq 0$) and equality ($\alpha_2 = 0$) simultaneously hold. We first proposed this condition in Ref. [18]. This is in fact an intermediate scenario, as shown in Fig. 2(d) for $\delta = 0.02$ eV, corresponding to the inner barrier of $Ga_{0.5}In_{0.5}As$ with $x = 0.5$ (see Table I). We find that α_1 is negative and consistently increases in magnitude with increasing V_g, as expected. In contrast to α_1, it is found that α_2 exhibits features of the sandwich geometry when $V_g < 0.135$ eV while it displays characteristics of the usual scenario when $V_g > 0.135$ eV. Note that α_2 identically vanishes at $V_g = 0.135$ eV, which can in principle be used as a handle for suppressing SO-induced spin relaxations for electrons of the second subband [44–46].

To explore further the underlying physics, in Fig. 3(c) [3(d)], we show α_1 (α_2) and its constituent contributions as functions of V_g. Ehrenfest's theorem [37,47] ensures $\langle \partial_z V \rangle_\nu = 0 = \langle \psi_\nu | \partial_z (V_w + V_g + V_d + V_e) | \psi_\nu \rangle$, from which the Rashba SO strength given in Eq. (6) can be rewritten as $\alpha_\nu = (1 - \eta_H/\eta_w)\alpha_\nu^w$. This indicates that if α_ν^w is zero α_ν must vanish, cf. α_2^w and α_2. Physically, we attribute the vanishing of α_2 to the *seeming* inversion symmetry *seen* solely by the second-subband electrons, due to a delicate cancellation of intrinsic and external SIAs induced by the inner barrier and the external gate, respectively. The inset of Fig. 3(d) shows that ψ_2 is essentially symmetric, even though ψ_1 is not.

F. Interband SO coupling

Figure 4(a) shows the gate dependence of the interband Rashba coupling. We find that η essentially remains constant with V_g. Note that the gate plus doping contribution (η^{g+d}) identically vanishes because of the orthogonality condition between ψ_1 and ψ_2. On the other hand, in the presence of the interband term, it is found that the spin branches of the two subbands may remain crossing [Fig. 4(b)] or become anticrossing [Fig. 4(c)], when the intraband α_1 and α_2 have the same and opposite signs, respectively. In either the crossing or the anticrossing scenario, the spin hybridization is not allowed, leaving the usual Rashba chiral spin texture unaltered; see the size (spin-polarization degree) and color (spin orientations) of markers in Figs. 4(b) and 4(c). For more details about the band dispersion and the spin texture, see the Supplemental Material [39]. Note that this is in contrast to the SO entanglement in the Rashba surface states of Bi/Ag(111) and Bi/Cu(111) [3,4], where physical phenomena related to orbital mixing occur, and is opposed to intriguing spin textures in 2DEG with both Rashba and Dresselhaus terms [12], where interband terms mix the two SO contributions.

G. Random Rashba term

Fluctuations of the concentration of dopant ions could lead to a random electric field along the growth direction

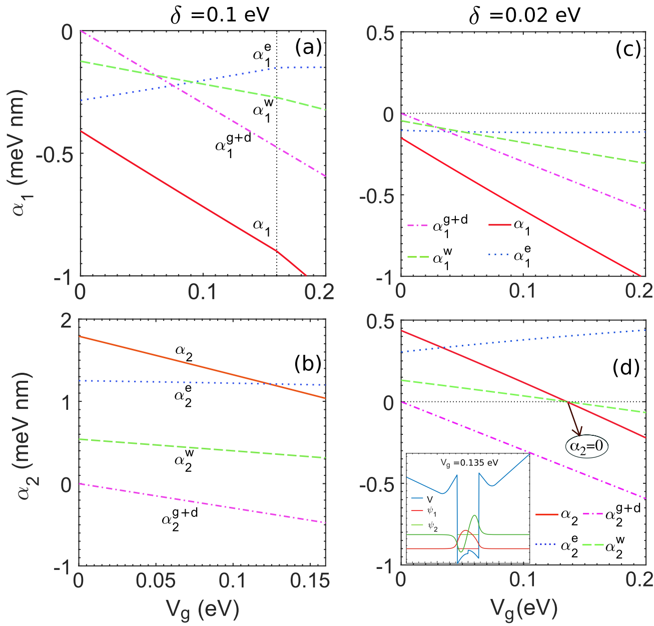

FIG. 3. Distinct contributions to Rashba SO strengths of the first (α_1) and second (α_2) subbands as functions of V_g, at $\delta = 0.1$ eV [panels (a) and (b)] and 0.02 eV [panels (c) and (d)]. In panel (a), the vertical dashed line at $V_g = 0.16$ eV marks a transition of the electron occupancy from two subbands to one subband. In panel (d), the inset shows a self-consistent outcome at $V_g = 0.135$ eV for which α_2 vanishes.

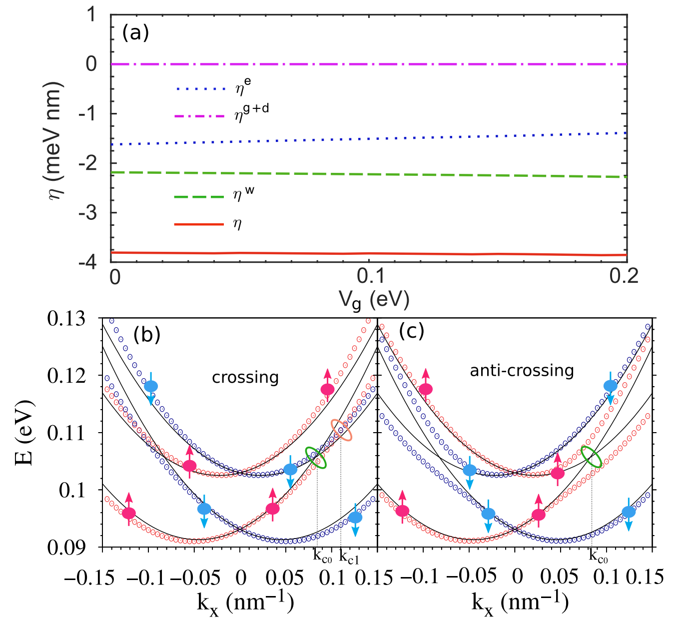

FIG. 4. (a) Intersubband Rashba coefficient η and its constituent contributions as functions of V_g. (c) Energy dispersions (scaled by a factor of 50 for visibility) along $k_x \parallel [100]$ of a AlInAs/GaInAs stepped well with $\delta = 0.1$ eV, for α_1 and α_2 having the same (c) and opposite (d) signs. The size of marker scales with the degree of spin polarization and the colors refer to spin orientations up (red, light) and down (blue, dark) indicated by up (down) arrows. The black lines correspond to the uncoupled ($\eta = 0$) bands which cross at k_{c0}. For $\eta \neq 0$, these bands remain crossing (a) with the crossing points shifted (cf. k_{c1} and k_{c0}) or exhibit anticrossing (b). The SO constants are chosen at $V_g = 0.1$ eV [see Fig. 2(d)] [35].

of quantum wells [48] and hence to a random Rashba coupling [48–52]. We follow Ref. [48] and evaluate the averaged random Rashba SO strength $\sqrt{\langle\alpha_R^2\rangle}$=$e^2\xi\sqrt{\pi n_d}/4\pi\epsilon R_d$, with the subscript R indicating the random contribution. Here e is the electron charge, ϵ denotes the dielectric constant, R_d refers to the distance from the doping region to the well center, and $\xi = \eta_H - \eta_w$ [13,18]. As electrons of the two subbands see the same doping conditions, fluctuations of the Rashba couplings are assumed to be the same in both subbands, i.e., $\sqrt{\langle\alpha_{1,R}^2\rangle}$=$\sqrt{\langle\alpha_{2,R}^2\rangle}$. For our stepped wells, the areal doping density reads $n_d \sim \rho_d l_d = 15 \times 10^{11}$ cm^{-2}, where $\rho_d = 2.5 \times 10^{18}$ cm^{-3} is the three-dimensional doping concentration and $l_d = 6$ nm stands for the length of doping layers. This yields a variation of the Rashba SO couplings $\sqrt{\langle\alpha_{\nu,R}^2\rangle}$~$0.3\alpha_\nu$. The random Rashba contribution may in reality modify the overall gate dependence of SO terms, while the basic feature of the opposite Rashba SO control in the sandwich geometry remains unaltered. Depending on specific applications, one can enhance (quench) the random Rashba effect by increasing (decreasing) the doping concentration and/or by setting the doping region near (distant from) the 2DEG region [Fig. 1(a)].

V. CONCLUDING REMARKS

We have considered ordinary GaInAs/AlInAs wells, which are widely adopted in experiments, and have in their stepped geometry captured fascinating SO features. In the scenario that the inner barrier is *sandwiched* between the two-subband energy levels, we have demonstrated opposite Rashba control. This opens a route towards selective and opposite SO control, greatly fascinating for spintronic applications, e.g., spin filters, the spin Hall effect, and spin transistors, with an extra pseudospin (subband) degree of freedom. This may also bring about the concept of *spin-subband locking*, despite a lack of direct protection from the time-reversal symmetry for *spin-valley locking* in 2D materials [9] and for *spin-momentum locking* in quantum-spin-Hall topological insulators [5]. Moreover, stepped wells with the sandwich geometry are expected to be preferable candidates of hosting topological matter of persistent skyrmion lattice [12] with the SO features conveniently controllable and Elliott-Yafet-like spin relaxation largely suppressible [53–55], due to a larger subband separation having the inner barrier in between. As a final remark, our recent report on stretchable spin helices demonstrated electrical control of the Dresselhaus term [13]. Additional work is needed to explore the feasibility of opposite Dresselhaus SO control.

ACKNOWLEDGMENTS

This work was supported by the National Natural Science Foundation of China (Grants No. 11874236 and No. 11004120) and the QFNU research fund.

[1] D. Awschalom, D. Loss, and N. Samarth, *Semiconductor Spintronics and Quantum Computation* (Springer, New York, 2002).
[2] I. Žutić, J. Fabian, and S. D. Sarma, Spintronics: Fundamentals and applications, Rev. Mod. Phys. **76**, 323 (2004).
[3] H. Bentmann, S. Abdelouahed, M. Mulazzi, J. Henk, and F. Reinert, Direct Observation of Interband Spin-Orbit Coupling in a Two-Dimensional Electron System, Phys. Rev. Lett. **108**, 196801 (2012).
[4] R. Noguchi, K. Kuroda, K. Yaji, K. Kobayashi, M. Sakano, A. Harasawa, T. Kondo, F. Komori, and S. Shin, Direct mapping of spin and orbital entangled wave functions under interband spin-orbit coupling of giant Rashba spin-split surface states, Phys. Rev. B **95**, 041111(R) (2017).
[5] B. A. Bernevig, T. L. Hughes, and S. C. Zhang, Quantum spin Hall effect and topological phase transition in HgTe quantum wells, Science **314**, 1757 (2006).
[6] R. M. Lutchyn, J. D. Sau, and S. Das Sarma, Majorana Fermions and a Topological Phase Transition in Semiconductor-Superconductor Heterostructures, Phys. Rev. Lett. **105**, 077001 (2010).
[7] Y. Oreg, G. Refael, and F. von Oppen, Helical Liquids and Majorana Bound States in Quantum Wires, Phys. Rev. Lett. **105**, 177002 (2010).
[8] H. Weng, C. Fang, Z. Fang, B. A. Bernevig, and X. Dai, Weyl Semimetal Phase in Noncentrosymmetric Transition-Metal Monophosphides, Phys. Rev. X **5**, 011029 (2015).
[9] D. Xiao, G. B. Liu, W. X. Feng, X. D. Xu, and W. Yao, Coupled Spin and Valley Physics in Monolayers of MoS_2 and Other Group-VI Dichalcogenides, Phys. Rev. Lett. **108**, 196802 (2012).
[10] J. Y. Fu, A. Bezerra, and F. Y. Qu, Valley dynamics of intravalley and intervalley multiexcitonic states in monolayer WS_2, Phys. Rev. B **97**, 115425 (2018).
[11] J. Y. Fu, J. M. R. Cruz, and F. Y. Qu, Valley dynamics of different trion species in monolayer WSe_2, Appl. Phys. Lett. **115**, 082101 (2019).
[12] J. Y. Fu, P. H. Penteado, M. O. Hachiya, D. Loss, and J. C. Egues, Persistent Skyrmion Lattice of Noninteracting Electrons with Spin-Orbit Coupling, Phys. Rev. Lett. **117**, 226401 (2016).
[13] F. Dettwiler, J. Y. Fu, S. Mack, P. J. Weigele, J. C. Egues, D. D. Awschalom, and D. M. Zumbühl, Stretchable Persistent Spin Helices in GaAs Quantum Wells, Phys. Rev. X **7**, 031010 (2017).
[14] P. J. Weigele, D. C. Marinescu, F. Dettwiler, J. Fu, S. Mack, J. C. Egues, D. D. Awschalom, and D. M. Zumbühl, Symmetry breaking of the persistent spin helix in quantum transport, Phys. Rev. B **101**, 035414 (2020).
[15] Y. A. Bychkov and E. I. Rashba, Properties of a 2D electron gas with lifted spectral degeneracy, JETP Lett. **39**, 78 (1984).
[16] G. Dresselhaus, Spin-orbit coupling effects in zinc blende structures, Phys. Rev. **100**, 580 (1955).
[17] M. P. Walser, U. Siegenthaler, V. Lechner, D. Schuh, S. D. Ganichev, W. Wegscheider, and G. Salis, Dependence of the Dresselhaus spin-orbit interaction on the quantum well width, Phys. Rev. B **86**, 195309 (2012).
[18] J. Y. Fu and J. C. Egues, Spin-orbit interaction in GaAs wells: From one to two subbands, Phys. Rev. B **91**, 075408 (2015).
[19] J. Nitta, T. Akazaki, H. Takayanagi, and T. Enoki, Gate Control of Spin-Orbit Interaction in an Inverted $In_{0.53}Ga_{0.47}As/In_{0.52}Al_{0.48}As$, Phys. Rev. Lett. **78**, 1335 (1997).
[20] M. Studer, G. Salis, K. Ensslin, D. C. Driscoll, and A. C. Gossard, Gate-Controlled Spin-Orbit Interaction in a Parabolic GaAs/AlGaAs Quantum Well, Phys. Rev. Lett. **103**, 027201 (2009).
[21] A. Sasaki, S. Nonaka, Y. Kunihashi, M. Kohda, T. Bauernfeind, T. Dollinger, K. Richter, and J. Nitta, Direct determination of spin-orbit interaction coefficients and realization of the persistent spin helix symmetry, Nat. Nanotechnol. **9**, 703 (2014).
[22] P. Chuang, S. Ho, L. W. Smith, F. Sfigakis, M. Pepper, C. Chen, J. Fan, J. P. Griffiths, I. Farrer, H. E. Beere, G. A. C. Jones, D. A. Ritchie, and T. Chen, All-electric all-semiconductor spin field-effect transistors, Nat. Nanotechnol. **10**, 35 (2015).
[23] H. C. Koo, J. H. Kwon, J. Eom, J. Chang, S. H. Han, and M. Johnson, Control of spin precession in a spin-injected field effect transistor, Science **325**, 1515 (2009).
[24] S. Datta and B. Das, Electronic analog of the electro-optic modulator, Appl. Phys. Lett. **56**, 665 (1990).
[25] J. Sinova, S. O. Valenzuela, J. Wunderlich, C. H. Back, and T. Jungwirth, Spin Hall effects, Rev. Mod. Phys. **87**, 1213 (2015).
[26] J. Wunderlich, B. Park, A. C. Irvine, L. P. Zârbo, E. Rozkotová, P. Nemec, V. Novák, J. Sinova, and T. Jungwirth, Spin Hall effect transistor, Science **330**, 1801 (2010).
[27] R. S. Calsaverini, E. Bernardes, J. C. Egues, and D. Loss, Intersubband-induced spin-orbit interaction in quantum wells, Phys. Rev. B **78**, 155313 (2008).
[28] J. Y. Fu, P. H. Penteado, D. R. Candido, G. J. Ferreira, D. P. Pires, E. Bernardes, and J. C. Egues, Spin-orbit coupling in wurtzite heterostructures, Phys. Rev. B **101**, 134416 (2020).
[29] W. Wang, X. M. Li, and J. Y. Fu, Electrical control of the spin-orbit coupling in GaAs from single to double and triple wells, Superlattices Microstruct. **88**, 43 (2015).
[30] Y. F. Hao, Spin-orbit interaction in multiple quantum wells, J. Appl. Phys. **117**, 013911 (2015).
[31] F. Nichele, M. Kjaergaard, H. J. Suominen, R. Skolasinski, M. Wimmer, B.-M. Nguyen, A. A. Kiselev, W. Yi, M. Sokolich, M. J. Manfra, F. Qu, A. J. A. Beukman, L. P. Kouwenhoven, and C. M. Marcus, Giant Spin-Orbit Splitting in Inverted InAs/GaSb Double Quantum Wells, Phys. Rev. Lett. **118**, 016801 (2017).
[32] D. Grundler, Large Rashba Splitting in InAs Quantum Wells Due to Electron Wave Function Penetration into the Barrier Layers, Phys. Rev. Lett. **84**, 6074 (2000).
[33] P. Kinsler, P. Harrison, and R. W. Kelsall, Intersubband electron-electron scattering in asymmetric quantum wells designed for far-infrared emission, Phys. Rev. B **58**, 4771 (1998).
[34] P. F. Yuh and K. L. Wang, Optical transitions in a step quantum well, J. Appl. Phys. **65**, 4377 (1989).
[35] The sign of α_1 is reversed for the band-crossing case.
[36] E. Q. Kane, Band structure of indium antimonide, J. Phys. Chem. Solids **1**, 249 (1957).
[37] R. Winkler, *Spin-Orbit Coupling Effects in Two-Dimensional Electron and Hole Systems* (Springer, New York, 2003).
[38] W. Wang, X. M. Li, and J. Y. Fu, Two distinct regimes for the electrical control of the spin-orbit interaction in GaAs wells, J. Magn. Magn. Mater. **411**, 84 (2016).

[39] See Supplemental Material at http://link.aps.org/supplemental/10.1103/PhysRevB.101.245403 for more details about the self-consistent procedure, effective 2D model, and spin texture, which includes Refs. [3,4,12,18,27,41].

[40] T. Koga, J. Nitta, T. Akazaki, and H. Takayanagi, Rashba Spin-Orbit Coupling Probed by the Weak Antilocalization Analysis in InAlAs/InGaAs/InAlAs Quantum Wells as a Function of Quantum Well Asymmetry, Phys. Rev. Lett. **89**, 046801 (2002).

[41] It is often called chemical potential μ in literature.

[42] I. Vurgaftman, J. R. Meyer, and L. R. Ram-Mohan, Band parameters for III-V compound semiconductors and their alloys, J. Appl. Phys. **89**, 5815 (2001).

[43] G. Bastard, *Wave Mechanics Applied to Semiconductor Heterostructures* (Halsted, Les Ulis, New York, 1989).

[44] N. S. Averkiev, L. E. Golub, and M. Willander, Spin relaxation anisotropy in two-dimensional semiconductor systems, J. Phys.: Condens. Matter. **14**, R271 (2002).

[45] M. D'yakonov, V. Marushchak, V. Perel', and A. Titkov, The effect of strain on the spin relaxation of conduction electrons in III-V semiconductors, Sov. Phys. JETP **63**, 655 (1986).

[46] T. D. Stanescu and V. Galitski, Spin relaxation in a generic two-timensional spin-orbit coupled system, Phys. Rev. B **75**, 125307 (2007).

[47] B. A. Lippmann, Ehrenfest's Theorem and Scattering Theory, Phys. Rev. Lett. **15**, 11 (1965).

[48] M. M. Glazov, E. Y. Sherman, and V. K. Dugaev, Two-dimensional electron gas with spin-orbit coupling disorder, Phys. E (Amsterdam, Neth.) **42**, 2157 (2010).

[49] M. M. Glazov and E. Y. Sherman, Nonexponential spin relaxation in magnetic fields in quantum wells with random spin-orbit coupling, Phys. Rev. B **71**, 241312(R) (2005).

[50] E. Y. Sherman, Random spin-orbit coupling and spin relaxation in symmetric quantum wells, Appl. Phys. Lett. **82**, 209 (2003).

[51] J. R. Bindel, M. Pezzotta, J. Ulrich, M. Liebmann, E. Y. Sherman, and M. Morgenstern, Probing variations of the Rashba spin-orbit coupling at the nanometre scale, Nat. Phys. **12**, 920 (2016).

[52] J. Nitta, Ready for a close-up, Nat. Phys. **12**, 898 (2016).

[53] S. Döhrmann, D. Hägele, J. Rudolph, M. Bichler, D. Schuh, and M. Oestreich, Anomalous Spin Dephasing in (110) GaAs Quantum Wells: Anisotropy and Intersubband Effects, Phys. Rev. Lett. **93**, 147405 (2004).

[54] R. J. Elliott, Theory of the effect of spin-orbit coupling on magnetic resonance in some semiconductors, Phys. Rev. **96**, 266 (1954).

[55] Y. Yafet, Conduction electron spin relaxation in the superconducting state, Phys. Lett. A **98**, 287 (1952).